Measurement 237 (2024) 115185

Contents lists available at ScienceDirect

Measurement

journal homepage: www.elsevier.com/locate/measurement

Upgrading the dynamic mathematical model of temperature sensors in gaseous media for low Biot number (Bi < 0.1)

Jorge Valencia-Santana [a,*], Alejandro Ramos-Martín [b], Vicente Henríquez-Concepción [b]

[a] University Institute of Intelligent Systems and Numerical Applications in Engineering, University of Las Palmas de Gran Canaria (ULPGC), 35017 Las Palmas de Gran Canaria, Spain
[b] Department of Process Engineering, University of Las Palmas de Gran Canaria (ULPGC), 35017 Las Palmas de Gran Canaria, Spain

ARTICLE INFO

Keywords:
Thermistor
Heat transfer
Transient response
Laplace Transform
Conduction losses

ABSTRACT

A mathematical model incorporating the transient response of NTC thermistors is presented. The internal thermal conduction resistance of the sensor relative to the thermal convection resistance of the medium results in a low Biot number ($Bi < 0.1$), yielding a fast dynamic response in gaseous media. This is advantageous in applications requiring minimal fluid interaction. However, negligible energy exchanges occur, introducing measurement uncertainty and ignoring the behavior of the measuring instrument. Therefore, this work proposes an improvement strategy for the mathematical model of these sensors, complementing the conventional model based on the concept of time constant. The strategy considers the heat flow through the thermistor wires in the energy balance, assuming they are semi-infinite solids and applying an approximation to the heat flow formula. Satisfactory improvement results were obtained compared to the conventional model, based on controlled laboratory tests with various gases.

1. Introduction

NTC thermistors are a popular choice for temperature measurement due to their accuracy, versatility, and ease of use compared to other transducers [1,2,3]. They offer several advantages over other temperature transducers including: high sensitivity, fast thermal response, a wide range of sizes and shapes and low cost [1,2,3,4].

Temperature measurements are used in various contexts, which can be classified as either stationary or transient phenomena [5]. In the case of stationary phenomena, a constant error or uncertainty is often observed [6]. In transient phenomena, the uncertainty or error associated with the measurement is typically variable and influenced by both the evolution of the phenomenon under study and the intrinsic characteristics of the temperature transducer or sensor [7], as illustrated in Fig. 1. This figure illustrates the dynamic response of a sensor $T_s(t)$ with a known time constant τ to periodic temperature variations of a gaseous medium, such as air, denoted as $T_g(t)$. So, $T_s(t)$ the temperature measured by the sensor, representing the ambient temperature. The analysis comprehensively considers airflow and including any associated errors $\left(T_g(t) - T_s(t)\right)$. To effectively deal with transient processes, it is crucial to use modelling strategies that consider the specific characteristics of the sensors or transducers used in their evaluation. This reduces measurement errors or uncertainties [8] and facilitates the isolation of the phenomenon under study.

The high dynamic response of NTC thermistors is partly due to their compact size, which facilitates efficient heat transfer between the sensor and its environment [9,10,11]. This relationship is commonly expressed by the dimensionless Biot number [12], which compares the sensor's internal thermal conduction resistance to its external thermal convection resistance. A low Biot number ($Bi < 0.1$) indicates that the internal thermal gradient of the sensor can be neglected [13], which is usually expressed as the dimensionless Biot number tends to zero. Therefore, it is assumed that the internal temperature of the sensor is uniform, resulting in a fast and accurate dynamic response in gaseous media. This assumption is conventionally applied in mathematical models that use the sensor time constant [14], which takes into account its mass, specific heat capacity, and the properties of the fluid, represented by the convection coefficient and the surface area of the sensor in contact with the gas. This paper discusses the limitations of a mathematical model based on the time constant for temperature sensors. The concept of the time constant is inherently linked to the characteristics of the medium in

* Corresponding author at: Engineering Building, Tafira Campus, 35017 Las Palmas de Gran Canaria, Spain.
E-mail addresses: jorge.valencia@ulpgc.es (J. Valencia-Santana), alejandro.ramos@ulpgc.es (A. Ramos-Martín), vicente.henriquez@ulpgc.es (V. Henríquez-Concepción).

https://doi.org/10.1016/j.measurement.2024.115185
Received 10 April 2024; Received in revised form 21 June 2024; Accepted 24 June 2024
Available online 24 June 2024

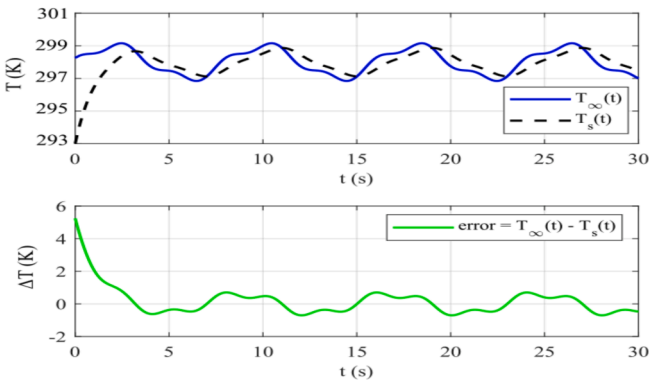

Fig. 1. Dynamic response of known time constant temperature sensor to sinusoidal temperature variation, including error.

which the sensor is situated and the physical properties of the sensor itself. These properties include thermal conductivity, heat capacity, the geometry of the sensor. This is of significant importance for the accuracy of models based on time constants, which implies different values of time constants depending on the gaseous medium in which it is immersed. Thus, these operation conditions arise due to the requirement of employing sensors that exhibit a synergy between the gaseous medium and the sensor, resulting in a low Biot number ($Bi < 0.1$). This primarily occurs in applications where there is minimal interaction with the phenomenon under study. In such scenarios, the influence of energy exchange through the sensor conductors can be likened to the energy interaction with the fluid being monitored and the surrounding environment of the gas confinement medium. The equations (1) and (2) below show the conventional model that illustrates the relationship between the time constant τ and the dimensionless Biot and Fourier numbers [12,15,16], (1) for a variable gas temperature $T_g(t)$ being $T_s(t)$ the sensor temperature, and (2) for a constant gas temperature T_g, where the sensor initial temperature is different from the gas temperature $T_s(0) \neq T_g$.

$$\tau\cdot\frac{dT_s(t)}{dt}+T_s(t)=T_g(t)\Rightarrow T_s(t)=e^{-\frac{t}{\tau}}\cdot\left[T_s(0)+\frac{1}{\tau}\cdot\int_0^t T_g(s)\cdot e^{\frac{s}{\tau}}ds\right]$$
$$\frac{1}{Bi}\cdot\frac{dT_s(Fo)}{dFo}+T_s(Fo)=T_g(Fo)\Rightarrow T_s(Fo)=e^{-Bi\cdot Fo}\cdot\left[T_s(0)+Bi\cdot\int_0^{Fo} T_g(s)\cdot e^{Bi\cdot s}ds\right] \quad (1)$$

$$\tau\cdot\frac{dT_s(t)}{dt}+T_s(t)=T_g\Rightarrow\frac{T_s(t)-T_g}{T_s(0)-T_g}=e^{-\frac{t}{\tau}}$$
$$\frac{1}{Bi}\cdot\frac{dT_s(Fo)}{dFo}+T_s(Fo)=T_g\Rightarrow\frac{T_s(Fo)-T_g}{T_s(0)-T_g}=e^{-Bi\cdot Fo} \quad (2)$$

As shown in (1) and (2), this model only takes into account the properties of the thermistor body and the surrounding fluid. The parameters used in this model are:$\tau = m_s\cdot c_{p_s}/h\cdot A_s$, $Bi = h\cdot L_c/k_s$, and $Fo = \alpha_s\cdot t/L_c^2$; where: m_s is the sensor mass, c_{p_s} the thermal specific capacity, h the heat transfer coefficient, L_c the characteristic sensor length, k_s the sensor thermal conductivity, α_s the sensor thermal difussivity, A_s the external sensor surface and finally, t is the time variable. It is suitable for various types of temperature sensors that meet the Biot number requirement ($Bi < 0.1$). Equations (1) and (2) represent a mathematical model that assumes an ideal scenario where only the exchange between the sensor and the fluid is considered, which is often referred to as lumped capacitance models [17]. However, in the case of a low Biot number ($Bi < 0.1$) situations, heat exchange through the thermistor wires connecting them to the corresponding circuit [18] can be significant. The dynamic response of the thermistor may be altered by this fact, which is not accounted for in the time constant model, (1) and (2).

However, this paper proposes an improvement to the model based on the time constant in which the heat flux exchanged through the thermistor wires is taken into account. The wires are assumed to behave as a semi-infinite solid [19]. In addition, an approach based on the use of equivalent transfer functions has been applied to the mathematical model of semi-infinite solids, which has been used with considerable success in several works [17,20]. The proposed model has been evaluated with experimental results and gives better results than the conventional time constant model. It is also relatively simple to use for the level of accuracy required.

The paper is structured as follows: Section 2 delineates the materials utilized in the experiments along with the methodological approach employed for data acquisition and processing. Section 3 elucidates the theoretical framework of the proposed model, encompassing the fundamental calculations underpinning the governing equations. The outcomes of the conducted tests are expounded upon in Section 4. These findings are subjected to critical analysis in Section 5 and ultimately, Section 6 deliberates upon the drawn conclusions.

2. Material and methods

A priori aim of this study is to replicate the response of a thermistor to an abrupt change in temperature using an external heat source generated by a laser. An experimental environment was meticulously designed, developed, and constructed to analyse the behaviour of these temperature sensors and to identify their operation conditions. The analysis was conducted within an experimental setup, as illustrated in Fig. 2, where the sensor is placed inside a fully insulated aluminium chamber, and a laser beam is projected onto the sensor to create a thermal stimulus. The interior of the chamber is configured to accommodate various gaseous media, including ambient air, helium, and even vacuum conditions. The wavelength of the laser significantly influences the power of the excitation signal, with power varying according to the frequency colour of laser. A laser generator capable of emitting different colours—purple (P), blue (B), red (R), and green (G)—was employed to provide a range of excitation powers. By varying the laser power and inducing different gaseous conditions within the chamber, it is possible to compare the sensor behaviours in ambient air, helium, and vacuum. Thus, the different laser powers are referred to as P, B, R, and G.

Table 1 shows some of the parameters that define the physical characteristics of the thermistor used in the tests (Part number: USP16673, Littelfuse). These values are for still air only, as the manufacturer has carried out the various tests under these conditions, as described in the general information on the NTC thermistor [21].

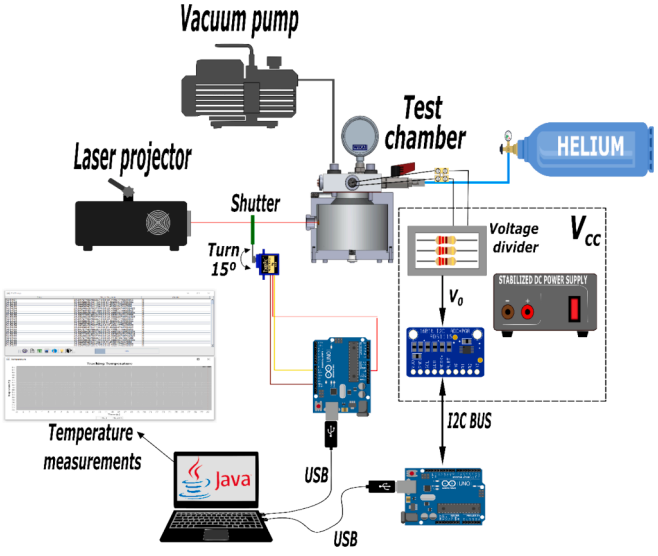

Fig. 2. Distribution of the test equipment.

Table 1
NTC thermistor manufacturer settings (Part number: USP16673, Littelfuse).

Parameter	Value
Resistance at 25 °C	10 kΩ ± 1 %
Nominal temperature	−30 °C to + 90 °C
β (25 °C to 85 °C)	3435 K nominal
Dissipation constant	0,7 mW/°C Nominal (still air)
Thermal time constant	5 s nominal (still air)

Furthermore, the table illustrates that the manufacturer has analysed the time constant for a specific fluid under defined conditions, resulting in the presented value. Nevertheless, the results of further tests with different fluids will demonstrate that this value is dependent on the properties of each fluid and the experimental conditions.

The configuration of the components in the proposed experiment is presented below using the schematic shown in Fig. 2. The data acquisition elements include: a voltage divider with two 10 kΩ resistors, a 16-bit analogue-to-digital converter (*ADS1115 Texas Instruments),* and two ATmega328 microcontrollers (*Atmel*) embedded in an Arduino system. One of these microcontrollers is used for data acquisition, while the other controls the laser shutter. Both boards are connected to a PC and communicate via an application developed specifically for the experiment, which allows the test bench actuator to be controlled, the data obtained to be managed and the measured temperature data to be monitored in real time.

On the other hand, humidity, pressure and light sensors are used to monitor other parameters inside the chamber. These devices are used for information purposes, as their measurements are used to check that there are no abrupt changes in the chamber during the tests.

With regard to the protocol to be followed in each test, it should be noted that the total duration is 180 s, during which three stages can be identified:

1. The first part is the rest period. This is important because it allows us to see if there are any disturbances that could affect the measurements to be taken. It lasts 30 s and during this time the temperature inside the chamber is measured before exposure to the laser. Taking into account that the microcontrollers used have a sampling frequency of 10 data per second, a total of 300 values are obtained. In this way, the average of the initial temperature is obtained, which allows the initial conditions to be established.
2. At the end of the first phase, the laser is activated and strikes the thermistor, starting the second phase of the test. In this part of the test, the transient response of the thermistor is observed. The total duration of this phase being 90 s from the moment the laser is activated.
3. Finally, the last phase of the test, lasting 60 s, corresponds to the return of the signal to the initial conditions after the laser has been switched off and the temperature has returned to its initial value.

In summary, this type of experiment provides information on the transient response of a diminutive temperature sensor in different environments in a controlled environment. It also allows a detailed analysis of what changes are produced by the energetic variation of the external signal and how this affects the measurements obtained. All this gas and energy exchange of the excitation signal allows analysis of whether the effects are mainly due to the medium or to the sensor cable assembly.

3. Theory and calculation

To model the dynamic response of a temperature sensor in a gaseous medium, an energy balance is used that takes into account energy interactions, as shown in the formula (3).

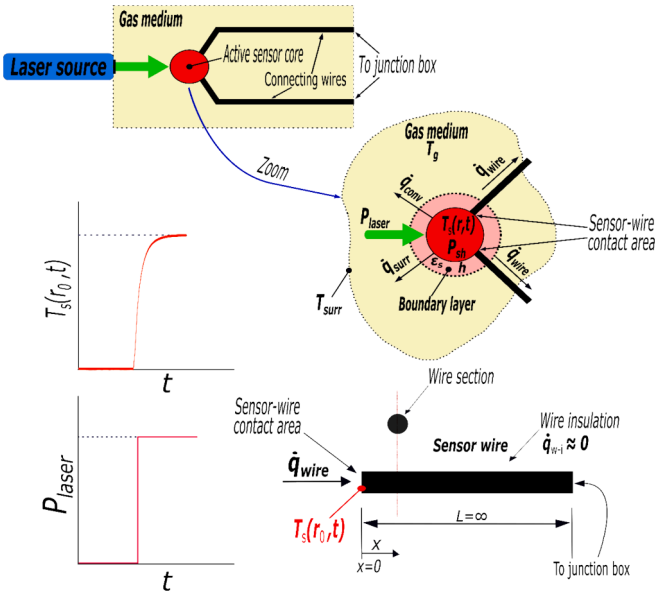

Fig. 3. Sensor schematic diagram.

$$P_{laser} - \dot{q}_{conv} - \dot{q}_{surr} - \dot{q}_{wire} = m_s \cdot c_{p_s} \cdot \frac{dT_s(t)}{dt} \tag{3}$$

The sensor, roughly assumed to be spherical in shape with radius r_0, is immersed in the gaseous medium and consists of a body (*core*), conductors and an excitation source, which is a laser acting as a thermal power source P_{laser}, as shown in Fig. 3.

Assuming a Biot number close to zero, a lumped capacitance model is established for the interaction of the sensor with the gaseous medium, with no temperature gradient inside the sensor and the temperature varying with time $T_s(t)$ [13,15,22]. As mentioned in the introduction, it is generally assumed that the dimensionless Biot number approaches zero for values less than 0.1. The accuracy of the mathematical model should increase as the dimensionless Biot number decreases. The Biot number (*Bi*) depends on the convection coefficient (*h*) of the fluid interface film in contact with the sensor surface. As the Biot number is proportional to the convection coefficient ($Bi = h \cdot D_s / k_s$), the value of Bi increases as h increases for the same sensor (diameter D_s and thermal conductivity sensor k_s are the same), simultaneously, this causes a decrease in the time constant $\tau = R_h \cdot C_1 = m_s \cdot c_p / h \cdot A_s$, due to its relation to h. Therefore, changing the gas in the test chamber will alter the *Bi* number and consequently affect the sensor's response. The energy balance proposed in (3) considers the incoming heat flux at the sensor surface, represented by P_{laser}, which remains constant over time. Additionally, it takes into account the heat transfer that is leaving the surface, which include convective exchange $\dot{q}_{conv}$ and radiative exchange $\dot{q}_{rad}$ with the internal surfaces of the test chamber. The equation (3) includes the heat losses through the sensor conductors and the variation of energy stored in the sensor per unit time, represented by the term $m_s \cdot c_p \cdot \mathrm{dT_s(t)/dt}$, where $C_1 = m_s \cdot c_p$ is the thermal capacity of the sensor (kJ/K). The upcoming analysis will examine each of the heat flows identified in equation (3) of the energy balance.

To determine the expression for the convective heat transfer ($\dot{q}_{conv}$) between the surface of the sensor and the gas in the medium in which it is immersed, certain considerations must be taken into account, as described below. The convective heat transfer is calculated according to Newton's cooling law (4),

$$\dot{q}_{conv} = h \cdot A_s \cdot (T_s - T_g) \tag{4}$$

where h is the average surface convection coefficient, which is related to the thermal behavior of the gas boundary layer surrounding the sensor

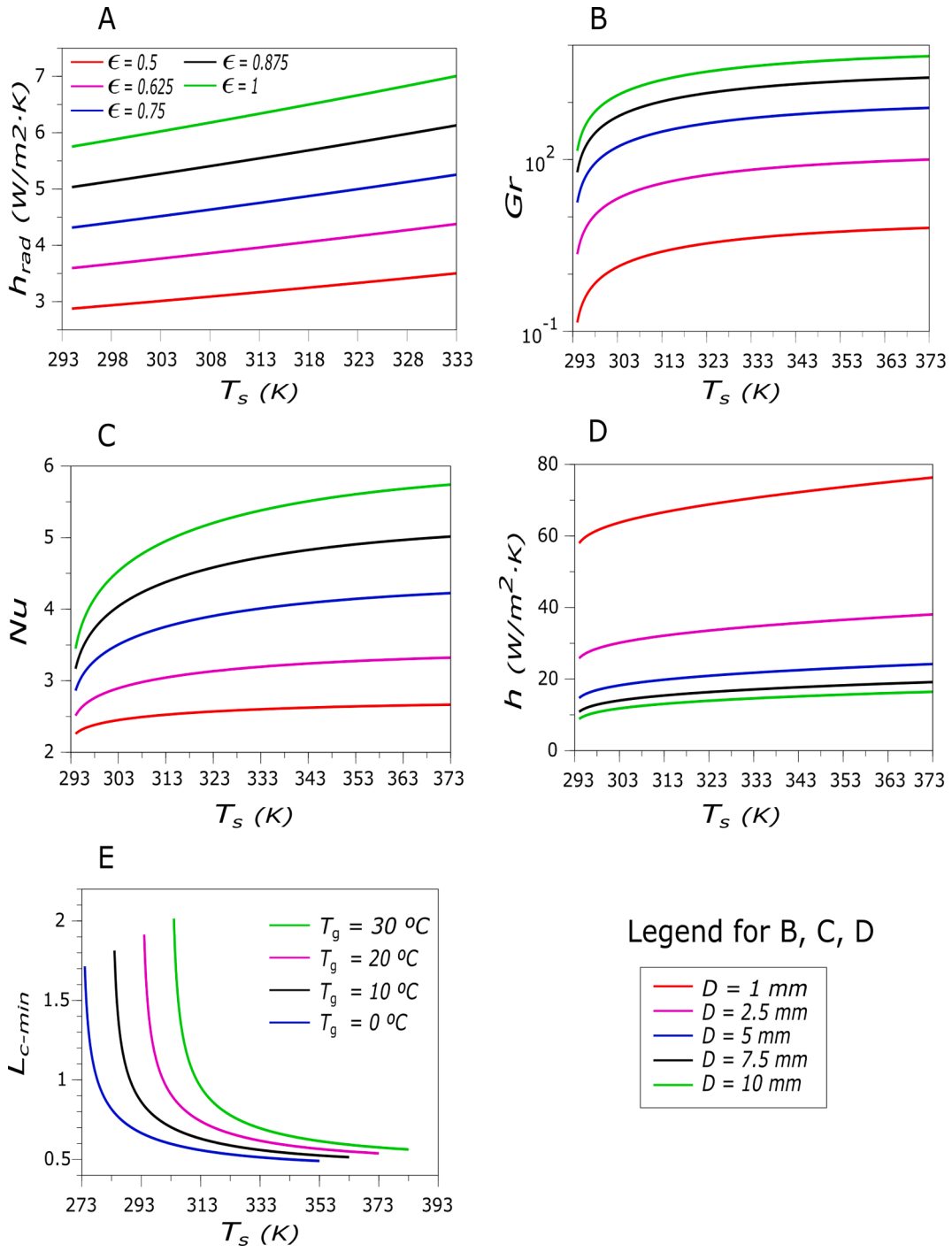

Fig. 4. Radiative and gas film properties for the sensor surface and air.

and acts as a proportionality factor to the temperature difference between the surface T_s and the gas T_g for the exchanged heat transfer $\dot{q}_{conv}$. The surface convection coefficient h depends on various factors, including fluid velocity, fluid regime, surface geometry, fluid type and whether the situation is stationary or transient. Regarding the topics explored in this paper, it must be taken into consideration that the different energy interactions indicated in the sensor will cause the temperature to vary over time, so that a transient phenomenon must be assumed, in which the influence of this condition on the variability of the surface convection coefficient must be analysed.

When a temperature difference exists between the sensor and the gaseous medium $|T_s(t) - T_g| \neq 0$, a fluid film or layer develops. This film has a common boundary with the sensor, i.e. the external surface of the sensor, through which a heat flow is exchanged between the sensor and the gaseous medium. This film considers a temperature gradient and the time required for its full development in transient processes. Heat transfer phenomena by conduction through the film predominate initially, followed by heat exchange by convection once developed, provided that the forces favouring fluid movement in the layer exceed those opposing it at a certain value. For free convection, buoyancy forces are in favour while viscous forces are opposed. In forced convection, inertia forces are favourable and viscous forces are opposed. The Grashof number (*Gr*) is typically used to distinguish this in free convection, while the Reynolds number (*Re*) is used in forced convection. These

parameters compare the forces that promote fluid motion with those that oppose it. When the dimensionless Grashof and Reynolds numbers are approximately equal to one ($Gr = 1$, $Re = 1$), heat transfer through the boundary layer is limited and occurs solely through conduction. The fluid movement in the boundary layer is considered to be zero. For the transient free convection situations studied in this paper, the surface convection coefficient (h) is presumed to remain constant, given the diminutive characteristic length L_c of the sensor, which assumes a spherical geometry ($L_c = D$), measuring only a few millimeters. Conversely, for modest temperature differentials between the sensor temperature (T_s) and the surrounding gas temperature (T_g), typically on the order of a few tens of degrees. This is found based on the expressions for estimating the surface convection coefficient h from the thermophysical properties of the gas (cinematic viscosity ν, thermal expansion coefficient β) obtained at the gas film temperature ($T_{film} = (T_s + T_g)/2$, where T_s is sensor temperature, and T_g is the gas temperature) and the appropriate experimental correlation for the given geometry, using the dimensionless Grashof (Gr) and Prandtl (Pr) numbers. One of the appropriate correlations for steady state free convection in sphere surfaces is the following (5):

$$Nu = 2 + \frac{0.589 \cdot Ra^{0.25}}{\left(1 + \left(\frac{0.469}{Pr}\right)^{9/16}\right)^{4/9}} \tag{5}$$

where the Nusselt number (Nu) is a dimensionless quantity that relates to the surface convection coefficient (h) through the relation $Nu = h \cdot L_c / k_g$, where L_c is the characteristic length of the sensor and k_g is the thermal conductivity of the gas. The Rayleigh number (Ra) is also dimensionless and can be calculated using the relation $Ra = Gr \cdot Pr$, where Gr is the dimensionless Grashof number, expressed as follows (6):

$$Gr = \frac{g \cdot \beta \cdot (T_s - T_g) \cdot L_c^3}{\nu \cdot \alpha} \tag{6}$$

Being g acceleration due to gravity, $\beta = 1/T_{film}$ the gas thermal expansion coefficient, L_c the characteristic length, ν the gas cinematic viscosity, α the gas thermal diffusivity.

From the Grashof (Gr) expression is possible to obtain a formula to estimate the minimum characteristic length, $L_{c\text{-min}}$, that must be considered for each situation can be determined when the condition is given that $Gr_{min} = 1$ (buoyancy forces and viscous forces in the boundary layer are equal), for a range of sensor temperature values T_s, for a fixed gas temperature T_g. The expression for $L_{c\text{-min}}$ (7) is given below and displayed in Fig. 4, Graph E, for air and various sensor diameter values, furthermore, graphs B, C and D, in the same figure, display the values for the Grashof number, Nusselt number and surface convection coefficient corresponding to the various diameters of the spherical sensor.

$$L_{c-min} = \left(\frac{\nu \cdot \alpha}{g \cdot \beta \cdot (T_s - T_g)}\right)^{1/3} \tag{7}$$

Therefore, if the diameter of the spherical sensor is of the same order as the minimum characteristic length, $D \approx L_{c-min}$, or even less, $D < L_{c-min}$, for the stationary case, it must be assumed that the exchange by conduction between the sensor surface and the gas around it will predominate. As a result, a practically constant surface convection coefficient should be assumed, as shown in graph D of Fig. 4, for the temperature range considered for the temperature sensor.

To estimate the heat transfer by radiation ($\dot{q}_{rad}$) between the surface of the sensor and the internal surface of the chamber, it is necessary to consider the surface emissivity of both the sensor and the chamber. For the purpose of this analysis, the chamber surface will be assumed to be ideal with an emissivity equal to one. The heat flow can be calculated using the expression (8) while taking into account the respective temperatures [12,15,16].

$$\dot{q}_{rad} = h_{rad} \cdot A_s \cdot (T_s - T_{surr}); h_{rad} = \epsilon_s \cdot \sigma \cdot \left(T_s^2 + T_{surr}^2\right) \cdot (T_s + T_{surr}) \tag{8}$$

Furthermore, a radiation coefficient (h_{rad}) is determined based on the indicated temperatures and the emissivity of the chamber surfaces. This coefficient is illustrated in graph A of Fig. 4, which displays a slight variation in the radiation coefficient, ranging from 5.7 to 7 $W/m^2 \cdot K$ when the surface emissivity is equal to one. Within the considered temperature range, it is possible to assume a constant value for the h_{rad} coefficient, which varies by 20 % from its minimum value, and approximately 2 % from the surface convection coefficient h, as demonstrated in graphs A and D of Fig. 4, which represents the worst-case scenario. As both coefficients h and h_{rad} are assumed to be constant and the gas and chamber surface temperature $T_g = T_{surr}$, an overall heat transfer coefficient (h_t) is considered that includes both convection and radiation effects, giving the expression of Newton's law of cooling, modified to include the effect of radiation, as shown in expression (9),

$$\dot{q}_t(t) = h_t \cdot A_s \cdot \left(T_s(t) - T_g\right) = \frac{T_s(t) - T_g}{R_h}; h_t = h + h_{rad} \tag{9}$$

where the expression for the calculation of the heat flux exchanged by convection and radiation across the sensor surface is provided.

Furthermore, considering that the wires are fully insulated, as seen in Fig. 3, and that there is no significant heat transfer to the environment, the analysis is focusing on the heat conduction along the wires. Thus, the analysis focuses on the heat transfer along the cable body, which could be modelled using the one-dimensional heat transfer equation. Thus, the one-dimensional ($1D$) heat transfer equation, assuming the semi-infinite solid hypothesis, can be a starting point to obtain the value of the transient temperature at the sensor surface, as confirmed by the studies in [23].

Consider the sensor wires as a semi-infinite solid with constant thermophysical properties, no internal heat generation, uniform thermal conditions over the exposed surface and initially a uniform temperature T_g over its entire length. The contact area between the sensor and the wires is considered to be the boundary of the semi-infinite medium $x = 0$ and the other end of the wires is considered to be at $x = \infty$, since an infinite length $L = \infty$ is assumed. Thus, the thermal conditions imposed on the surface of the sensor are determined by the heat conduction of a semi-infinite solid and therefore the solution is strongly dependent on the boundary conditions set at $x = 0$, which coincide with the imposition of the temperature at which the sensor is located. However, once the change of variable $\theta(x,t) = T(x,t) - T_g$ has been introduced and the initial and boundary conditions have been established, the differential equation for heat conduction in conductors is as follows [12,15,16]:

$$\frac{\partial^2 \theta(x,t)}{\partial x^2} = \frac{1}{\alpha_w} \cdot \frac{\partial \theta(x,t)}{\partial t} \tag{10}$$

Boundary condition $.x = 0; \theta(0,t) = T_s(t) - T_g$

Boundary condition $.x = \infty; \theta(\infty,t) = T_s(t) - T_g = 0$

Initial condition $.t = 0; \theta(x,0) = 0$

where α_w is the thermal diffusivity of the cable material, $\alpha_w = k_w/(\rho_w \cdot c_{p_w})$, k_w is the thermal conductivity, ρ_w is the density, and c_{p_w} is the specific heat capacity.

Applying the Laplace transform [17,24,25] to equation (10), it is obtained the following differential equation (11):

$$\frac{\partial^2 \theta(x,s)}{\partial x^2} = \frac{1}{\alpha_w} \cdot s \cdot \theta(x,s) \tag{11}$$

Boundary condition $.x = 0; \theta(0,s) = T_s(s) - T_g$

Boundary condition $.x = \infty; \theta(\infty,s) = 0$

This differential equation is linear homogeneous. And its solution is given in (12).

$$\theta(x,s) = C_1 \cdot e^{-\sqrt{\frac{s}{\alpha_w}}x} + C_2 \cdot e^{\sqrt{\frac{s}{\alpha_w}}x} \tag{12}$$

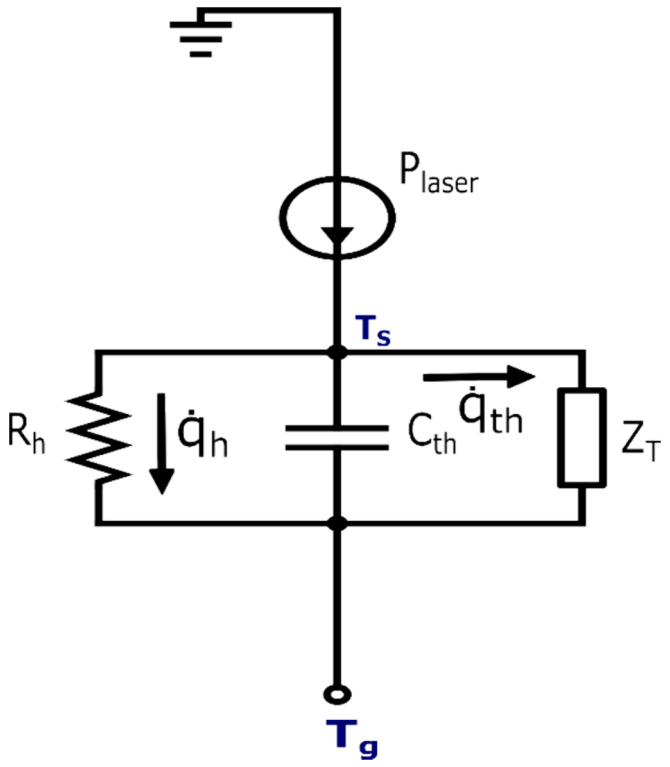

Fig. 5. Impedance modelling equivalent electrical diagram for our proposal.

Starting from the condition $\theta(\infty,s) = 0$, from which it follows that $C_2 = 0$, the solution (12) has the form:

$$\theta(x,s) = C_1 \cdot e^{-\sqrt{\frac{s}{\alpha_w}}x} \tag{13}$$

Thus, the boundary condition for $x = 0$ determines the constant C_1, leaving the solution in (14).

$$\theta(x,s) = \frac{\theta(0,s)}{s} \cdot e^{-\sqrt{\frac{s}{\alpha_w}}x} \tag{14}$$

To obtain an expression for the heat flow through the cables, the Fourier law must be applied to the expression (14) and then evaluated at $x = 0$, as shown in (15). On the other hand, considering the initial condition $\theta(x,0) = 0$ and Fourier's law: $-k_w \cdot A_w \cdot \frac{d\theta(x,s)}{dx}\Big|_{x=0} = \dot{q}_w(s)$, equation (14) would be as shown in (15), given that the cable cross section is A_w through which the heat flow of the cables passes.

$$\dot{q}_w(s) = \dot{q}(0,s) = -k_w \cdot A_w \cdot \frac{d\theta(x,s)}{dx}\Big|_{x=0} = \frac{k_w}{\sqrt{\alpha_w}} \cdot A_w \cdot \sqrt{s} \cdot \theta(0,s) \tag{15}$$

Given that $\theta(0,s) = T_s(s) - T_g$, an expression for the heat flow through the wires is obtained from the sensor temperature in (16).

$$\dot{q}_w(s) = \frac{k_w}{\sqrt{\alpha_w}} \cdot A_w \cdot \sqrt{s} \cdot \theta(0,s) = \frac{k_w}{\sqrt{\alpha_w}} \cdot A_w \cdot \sqrt{s} \cdot \left(T_s(s) - T_g\right) \tag{16}$$

At this point, all the elements of the energy balance (3) have been defined, which can be rewritten in the complex (Laplace) field as shown in (17), taking into account that $dT_s(t)/dt = d\left(T_s(t) - T_g\right)/dt$, since T_g is constant.

$$\frac{P_{laser}}{s} - \dot{q}_t(s) - \dot{q}_w(s) = m_s \cdot c_{p_s} \cdot s \cdot \left(T_s(s) - T_g\right) \tag{17}$$

In equation (17), the different heat flows determined in (9) and (16) can be substituted, resulting in equation (18).

Table 2
Coefficient values for (19) and (20).

	$Z_1(s)$	$Z_2(s)$
a_0	3	5
a_1	1	10
a_2	–	1
b_1	3	10
b_2	–	5

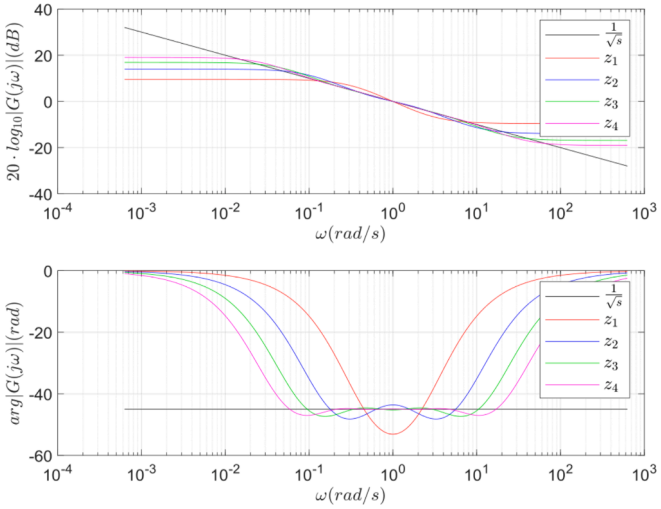

Fig. 6. Bode diagrams.

$$\frac{P_{laser}}{s} - \frac{T_s(s) - T_g}{R_h} - \frac{k_w}{\sqrt{\alpha_w}} \cdot A_w \cdot \sqrt{s} \cdot \left(T_s(s) - T_g\right) = m_s \cdot c_{p_s} \cdot s \cdot \left(T_s(s) - T_g\right) \tag{18}$$

By applying the inverse Laplace transform to equation (18), a mathematical expression for determining the sensor temperature $\left(T_s(s) - T_g\right)$ could be obtained from the exposure to the constant laser power (P_{laser}), taking into account the inclusion of the heat flow through the sensor conductors. Equation (18) can be represented by its electrical analogue shown in Fig. 5 [24], where the laser action is associated with a constant current source P_{laser}/s, the total heat flux by convection and radiation is represented as a thermal resistance (R_h) in parallel with a heat capacity associated with the sensor core $C_1 = m_s \cdot c_{p_s}$ and as such capacity is influenced by the complex operator s, which corresponds to the derivative in the time field $\left(L^{-1}[s \cdot F(s)] = df(t)/dt - f(0)\right)$. Finally, also in parallel, another branch related to a thermal impedance associated with the sensor wires and affected by the square root of the operator s, thus $\sqrt{s} \cdot \theta(s)$. Real-world problems with equations similar to equation (18) are easily solved when the exponents of the s operator are of integer order [26], leaving any other situation to solutions obtained from approximations of the corresponding transfer functions. In this article we propose an approximation method with equivalent transfer functions for the $\sqrt{s}$ operator, which can be used to solve equation (18). The proposed approximation method is based on the work of Carlson and Halijak [27], who considered the problem as an approximation by a regular Newton process.

Thus, using the method developed by Carlson [28,29,30], it is obtained a rational approximation based on transfer functions for different functions in the complex field, as well as for the irrational operator $\sqrt{s}$ shown by (19) and (20).

$$\frac{1}{\sqrt{s}} \approx Z_1(s) = \frac{a_1 \cdot s + a_0}{b_1 \cdot s + 1} \tag{19}$$

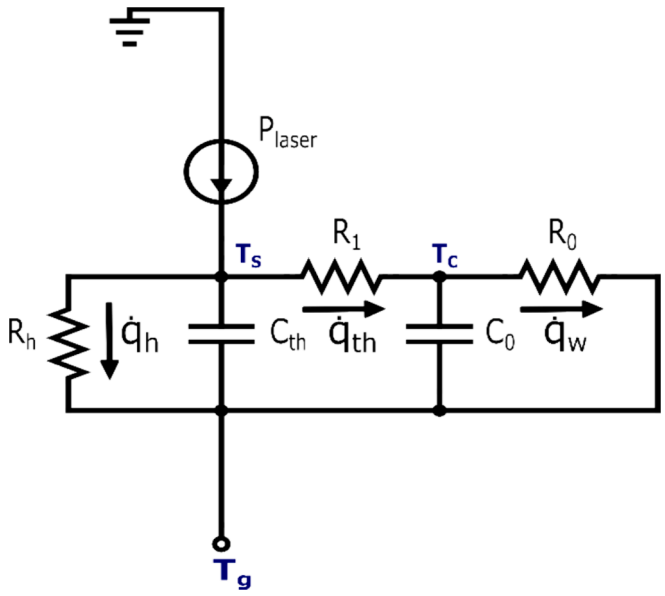

Fig. 7. Equivalent circuit diagram for the simplified model.

$$\frac{1}{\sqrt{s}} \approx Z_2(s) = \frac{a_2 \cdot s^2 + a_1 \cdot s + a_0}{b_2 \cdot s^2 + b_1 \cdot s + 1} \tag{20}$$

Table 2 shows the values of the coefficients for (19) and (20). These are obtained by applying Carlson's method [28,29,30].

As can be seen in (19) and (20), the approximations are transfer functions with polynomials of the same order for the numerator and denominator. Using the method developed by Carlson [28,29,30], it was possible to obtain equivalent transfer functions of higher order, with polynomials of order 2, 3, …, with a corresponding improvement in the approximations made. Fig. 5 shows the effect of these approximations on the theoretical behaviour of the $\sqrt{s}$ operator, with a better fit as the order of the polynomials increases, as can be seen from the Bode plots in Fig. 6.

However, as the number of elements increases, it can become computationally expensive and require a more detailed analysis of the boundary conditions and thermal properties of the system, which may not always be necessary. For this reason, it has been decided to use an approach that reduces the level of complexity and provides appropriate solutions.

On the other hand, the approximation of the proposed $\sqrt{s}$ operator allows a generic view of the thermal system. Thus, Fig. 7 shows an equivalent circuit with the $Z_1(s)$ approximation of the electrical analogue of the thermal problem, where the following elements are considered total resistance $R_h = R_{conv} + R_{rad}$, heat capacity of the thermistor C_1, convective and radiative heat flux $\dot{q}_t$ through the resistor R_h, heat flux through the wires $\dot{q}_1$ and $\dot{q}_0$, heat capacity of the conductors C_0, thermal resistances associated with the conductors (R_1 and R_0). The contribution of the equivalent impedance $Z_1(s)$ in Fig. 7 is observed in its equivalent branch corresponding to the set of elements R_1, C_0 and R_0, i.e. two thermal resistances and one thermal capacity, in the same way as for the case of $Z_2(s)$, it would be three thermal resistances and two thermal capacities. It should be noted that in order to describe a model under vacuum conditions, as will be discussed later, the term R_h tends to infinity, so it disappears.

Therefore, the total impedance of the thermal diagram shown in Fig. 7 is obtained by considering the parallel connection of the resistance R_h, the capacitance C_1 and the impedance $Z^*_1(s)$, and it is displayed in (21).

$$Z_T(s) = \frac{R_h \cdot Z_1^*(s)}{R_h + (R_h \cdot C_1 \cdot s + 1) \cdot Z_1^*(s)} \tag{21}$$

where the term $Z_1^*(s) = \left(\frac{k_w}{\sqrt{\alpha_w}} \cdot A_w\right)^{-1} \cdot Z_1(s)$, which is displayed in (22).

$$Z_1^*(s) = \left(\frac{k_w}{\sqrt{\alpha_w}} \cdot A_w\right)^{-1} \cdot \frac{C_0 \cdot R_0 \cdot R_1 \cdot s + R_0 + R_1}{C_0 \cdot R_0 \cdot s + 1} \approx \left(\frac{k_w}{\sqrt{\alpha_w}} \cdot A_w\right)^{-1} \cdot \frac{1}{\sqrt{s}} \tag{22}$$

The expression to obtain the temperature difference experienced by the sensor as a function of the external excitation source is expressed by (23) in the Laplace domain.

$$\theta(s) = \left(T_s(s) - T_g\right) = \frac{P_{laser}}{s} \cdot Z_T(s) \tag{23}$$

Expression (23) can be expressed as shown in (24) for the case when all heat flows $\left(\dot{q}_t = \dot{q}_{conv} + \dot{q}_{rad}, \dot{q}_w\right)$ are considered.

$$\theta_1(s) = \frac{a}{s} \cdot \frac{s + 3}{b \cdot s^2 + (3 \cdot (1 + b) + c) \cdot s + 3 \cdot c + 1} \tag{24}$$

If the heat flow by convection and radiation is not taken into account, the expression (25) is obtained in the case of a vacuum in the test chamber.

$$\theta_2(s) = \frac{a}{s} \cdot \frac{s + 3}{b \cdot s^2 + 3 \cdot (1 + b) \cdot s + 1} \tag{25}$$

where $a = P_{laser} \cdot \left(A_w \cdot k_w / \sqrt{\alpha_w}\right)^{-1}$, $b = C_{th} \cdot \left(A_w \cdot k_w / \sqrt{\alpha_w}\right)^{-1}$, and $c = \left(R_h \cdot A_w \cdot k_w / \sqrt{\alpha_w}\right)^{-1}$. For the conventional model (26), with no heat flow through the wires, it is obtained that $a^* = P_{laser} \cdot R_h$, $b^* = \tau = C_{th} \cdot R_h$.

$$\theta_3(s) = \frac{a^*}{s} \cdot \frac{1}{b^* \cdot s + 1} = \frac{a^*}{s} \cdot \frac{1}{\tau \cdot s + 1} \tag{26}$$

By applying the inverse Laplace transform and making the appropriate groupings, the expression for the temperature response experienced by the thermistor after the external laser excitation source is obtained for expressions (27), (28) and (29).

$$\theta_1(t) = \epsilon_1 + \lambda_1 \cdot e^{-(\delta_1 + \gamma_1) \cdot t} - (\epsilon_1 + \lambda_1) \cdot e^{-(\delta_1 - \gamma_1) \cdot t} \tag{27}$$

$$\theta_2(t) = \epsilon_2 + \lambda_2 \cdot e^{-(\delta_2 + \gamma_2) \cdot t} - (\epsilon_2 + \lambda_2) \cdot e^{-(\delta_2 - \gamma_2) \cdot t} \tag{28}$$

$$\theta_3(t) = a^* \cdot \left(1 - e^{-t/\tau}\right) = a^* \cdot \left(1 - e^{-Bi \cdot Fo}\right) \tag{29}$$

The model parameters are presented in Table 3.

Bearing in mind that, in the stationary regime and assuming that $T_s(0) = T_g$, for $t = \infty$, it is obtained that $\theta_i(\infty)$ is:

Table 3
Parameters for the expressions (27) and (28).

	ϵ_i	λ_i	δ_i	γ_i
$\theta_1(t)$	$\frac{3 \cdot a}{3 \cdot c + 1}$	$\frac{3 \cdot a}{3 \cdot c + 1} \cdot \left(\frac{3}{2 \cdot \delta_1} - \frac{1}{2} \cdot \frac{\gamma_1}{\delta_1} + \frac{4}{3 \cdot b \cdot \delta_1} - \frac{1}{2}\right)$	$\frac{\sqrt{9 \cdot b^2 + 14 \cdot b + 9 - 6 \cdot b \cdot c + 6 \cdot c + c^2}}{2 \cdot b}$	$\frac{c}{2 \cdot b} + \frac{3}{2 \cdot b} + \frac{3}{2}$
$\theta_2(t)$	$3 \cdot a$	$\frac{a}{2 \cdot \delta_2} + \frac{7 \cdot a}{6} \cdot \frac{\gamma_2}{\delta_2} - \frac{3 \cdot a}{2}$	$\frac{\sqrt{9 \cdot b^2 + 14 \cdot b + 9}}{2 \cdot b}$	$\frac{3}{2 \cdot b} + \frac{3}{2}$

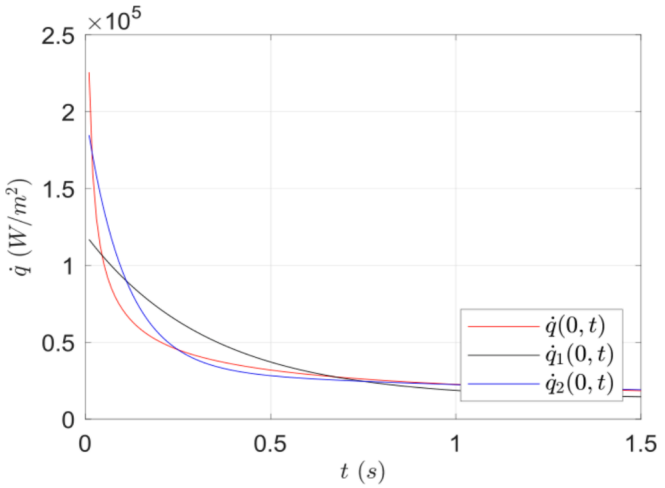

Fig. 8. Heat flow for constant temperature T_s at $x = 0$.

$$\theta_i(\infty) = T_s(\infty) - T_g = \epsilon_i \rightarrow \begin{cases} T_s(\infty) = \epsilon_i - T_s(0) \\ \theta_i(\infty) = T_s(\infty) - T_s(0) \end{cases}; i = \{1,2\} \tag{30}$$

Taking into account that $T_g = T_s(0)$, expressions (27) and (28) are expressed as (32).

$$\frac{T_s(t) - T_s(\infty)}{T_s(0) - T_s(\infty)} = -\frac{\lambda_i}{\epsilon_i} \cdot e^{-(\delta_i+\gamma_i)\cdot t} + \left(1 + \frac{\lambda_i}{\epsilon_i}\right) \cdot e^{-(\delta_i-\gamma_i)\cdot t}; i = \{1,2\} \tag{31}$$

$$\Theta_i(t) = -\frac{\lambda_i}{\epsilon_i} \cdot e^{-(\delta_i+\gamma_i)\cdot t} + \left(1 + \frac{\lambda_i}{\epsilon_i}\right) \cdot e^{-(\delta_i-\gamma_i)\cdot t}; i = \{1,2\} \tag{32}$$

For $\theta_3(t)$ the same change can be made obtaining (33).

$$\Theta_3(t) = e^{-t/\tau} = e^{-Bi \cdot Fo} \tag{33}$$

where $\theta(\infty) = a^*$. Where $\Theta_1(t)$, $\Theta_2(t)$, and $\Theta_3(t)$ represent temperatures in dimensionless form.

This proposal can be approached using the quadrupole method [17], which is particularly suitable for solving 1D transient heat transfer problems in complex systems. This method is especially useful when dealing with systems that have complex geometries or varying boundary conditions.

3.1. Calculations for the proposed model

This section presents calculations and results obtained from the approximations proposed in (18) and (19) for specific boundary conditions that have an analytical solution. These results will demonstrate the suitability and scope of the proposals for the problem evaluated in this article. Starting from the analytical solution of equation (10), an inverse Laplace transformation is applied for a step temperature of $\theta(0,s) = (T_s - T_g)/s = \theta/s$ at $x = 0$, where T_s is assumed to be constant [16]. The analytical solution of (17) is shown in expression (33) for the considered conditions.

$$\begin{aligned} \dot{q}(0,s) &= \sqrt{\rho \cdot c_p \cdot k} \cdot \sqrt{s} \cdot \frac{\theta}{s} = \sqrt{\rho \cdot c_p \cdot k} \cdot \frac{\theta}{\sqrt{s}} \xrightarrow{L^{-1}[\dot{q}(0,s)]} \dot{q}(0,t) \\ &= \frac{k}{\sqrt{\pi \cdot \alpha \cdot t}} (T_s - T_g) \end{aligned} \tag{34}$$

Equations (35) and (36) can be used to approximate the analytical heat flux expressed in (34). These equations were obtained by applying the inverse Laplace transform, taking into account the step input and the approximations $Z_1(s)$ and $Z_2(s)$, respectively.

$$\dot{q}_1(0,t) \approx -\frac{k}{\sqrt{\alpha}} \cdot L^{-1}\left[\theta(0,s) \cdot z_1{}^{-1}(s)\right] = -\frac{k}{\sqrt{\alpha}} \cdot L^{-1}\left[\frac{\theta}{s} \cdot z_1{}^{-1}(s)\right]$$

$$\dot{q}_1(0,t) \approx -\frac{k}{3 \cdot \sqrt{\alpha}} \cdot (T_s - T_g) \cdot (8 \cdot e^{-3 \cdot t} + 1) \tag{35}$$

$$\dot{q}_2(0,t) \approx -\frac{k}{\sqrt{\alpha}} \cdot L^{-1}\left[\theta(0,s) \cdot z_2{}^{-1}(s)\right] = -\frac{k}{\sqrt{\alpha}} \cdot L^{-1}\left[\frac{\theta}{s} \cdot z_2{}^{-1}(s)\right]$$

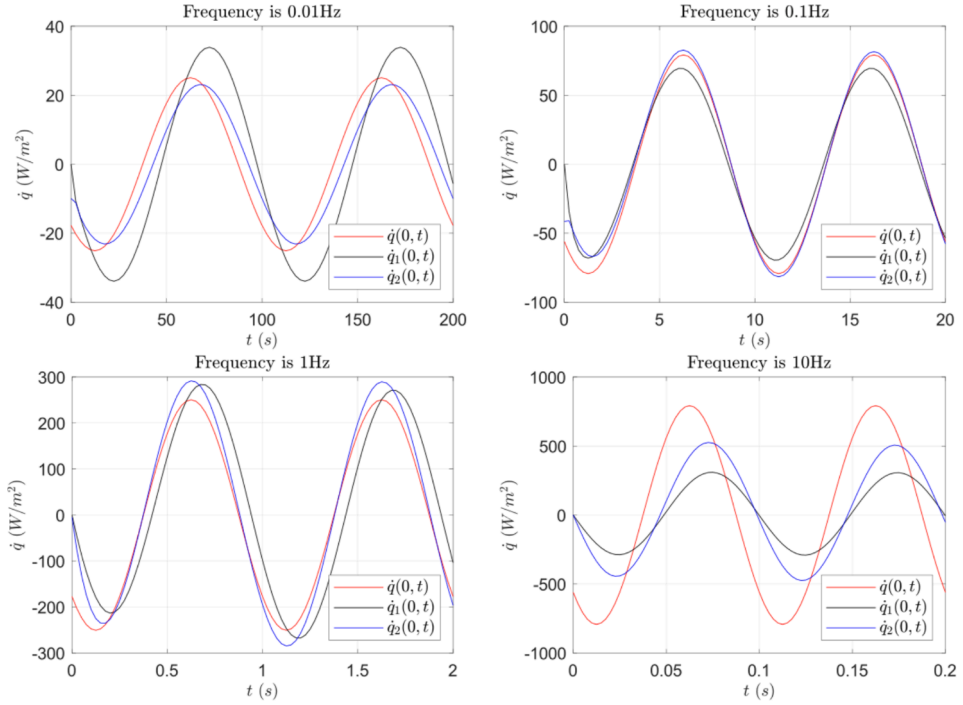

Fig. 9. Periodic signal heat flow.

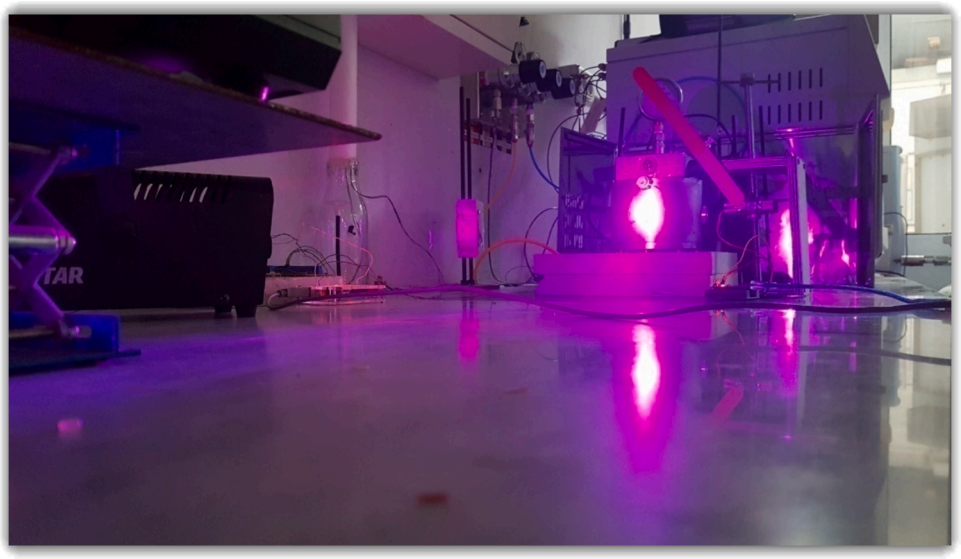

Fig. 10. Practical test to evaluate the transient response of the thermistor under the highest power signal.

$$\dot{q}_2(0,t) \approx -\frac{k}{5\cdot\sqrt{\alpha}}\cdot(T_s - T_g)\cdot\left(1 + 4\cdot\left(3+\sqrt{5}\right)\cdot e^{\left(-5-2\cdot\sqrt{5}\right)\cdot t} + 4\cdot\left(3 - \sqrt{5}\right)\cdot e^{\left(-5+2\cdot\sqrt{5}\right)\cdot t}\right) \tag{36}$$

Fig. 8 displays the results of the approximations (35) and (36) for a temperature step of $\theta = 1^oC$ with a thermal conductivity of $k = 400W/m\cdot^oC$ and a thermal diffusivity of $\alpha = 100\cdot10^{-6}m^2/s$, as well as the outcome of the analytical solution (34). It can be observed that the approximations are sufficiently accurate, particularly as time progresses beyond half a second, for an abrupt temperature change at $x = 0$ (step temperature input).

This discussion considers the second case for the analytical solution of equation (10), which involves applying a periodic temperature of the form presented in (36) at $x = 0$. The analytical solution for (10) under these conditions is given in expression (38).

$$\theta(0,t) = \Delta T\cdot sin(\omega\cdot t) \tag{37}$$

$$\dot{q}(0,t) = k\cdot A\cdot\Delta T\cdot\sqrt{\frac{\omega}{\alpha}}\cdot sin\left(\omega\cdot t + \frac{\pi}{4}\right) \tag{38}$$

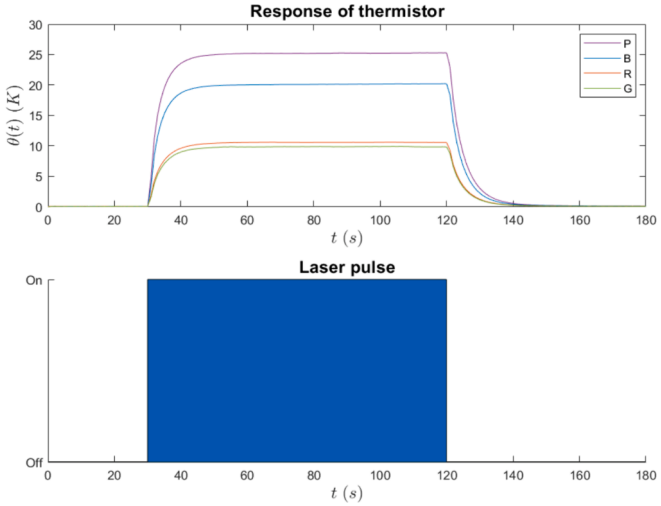

Fig. 11. Thermistor response to ambient air in chamber.

Expressions (39) and (40) can be used to approximate the analytical heat flux expressed in (38). These equations were obtained by applying the inverse Laplace transform, taking into account the periodic temperature input and the approximations $Z_1(s)$ and $Z_2(s)$, respectively.

$$\dot{q}_1(0,t) \approx -\frac{k}{\sqrt{\alpha}}\cdot\Delta T\cdot\omega\cdot L^{-1}\left[\frac{1}{s^2+\omega^2}\cdot {z_1}^{-1}(s)\right]$$

$$\dot{q}_1(0,t) \simeq -\frac{k}{\sqrt{\alpha}}\cdot\frac{\Delta T\cdot\omega}{\omega^2+9}\cdot\left(-8\cdot e^{-3\cdot t} + 3\cdot\left(\omega+\frac{1}{\omega}\right)\cdot sin(\omega\cdot t) + 8\cdot cos(\omega\cdot t)\right) \tag{39}$$

$$\dot{q}_2(0,t) \approx -\frac{k}{\sqrt{\alpha}}\cdot\Delta T\cdot\omega\cdot L^{-1}\left[\frac{1}{s^2+\omega^2}\cdot {z_2}^{-1}(s)\right]$$

$$\dot{q}_2(0,t) \simeq -\frac{k}{5\cdot\sqrt{\alpha}}\cdot\frac{\Delta T}{\omega^4+90\cdot\omega^2+25}\cdot\Big[\Big(-\left(44\cdot\sqrt{5}+100\right)\cdot\omega^3 + \left(20\cdot\sqrt{5}+100\right)\cdot\omega\Big)\cdot e^{\left(-5-2\cdot\sqrt{5}\right)\cdot t} + \Big(\left(44\cdot\sqrt{5}-100\right)\cdot\omega^3 - \left(20\cdot\sqrt{5}+100\right)\cdot\omega\Big)\cdot e^{\left(-5+2\cdot\sqrt{5}\right)\cdot t} + \left(25\cdot\omega^4 + 370\cdot\omega^2 + 25\right)\cdot sin(\omega\cdot t) + \left(200\cdot\omega^3 + 200\cdot\omega\right)\cdot cos(\omega\cdot t)\Big] \tag{40}$$

Fig. 9 displays the results of the approximations (39) and (40) for a sinusoidal temperature of $\Delta T = 1^oC$ amplitude and for different angular frequencies, with a thermal conductivity of $k = 400W/m\cdot^oC$ and a thermal diffusivity of $\alpha = 100\cdot10^{-6}m^2/s$, as well as the outcome of the analytical solution (38). The approximations are observed to be sufficiently accurate, particularly for frequencies of 0.1 and 1 Hz. These frequencies fall within the range where approximations (39) and (40) align most closely with $1/\sqrt{s}$, as evidenced by the Bode diagrams in Fig. 6.

4. Results

The following section presents the response of a thermistor to an external heat source, specifically a power laser, in various gaseous media. The data is presented in a format that allows for the results obtained in ambient air, helium, and vacuum conditions to be easily compared. Similarly, the tables displaying model parameters and

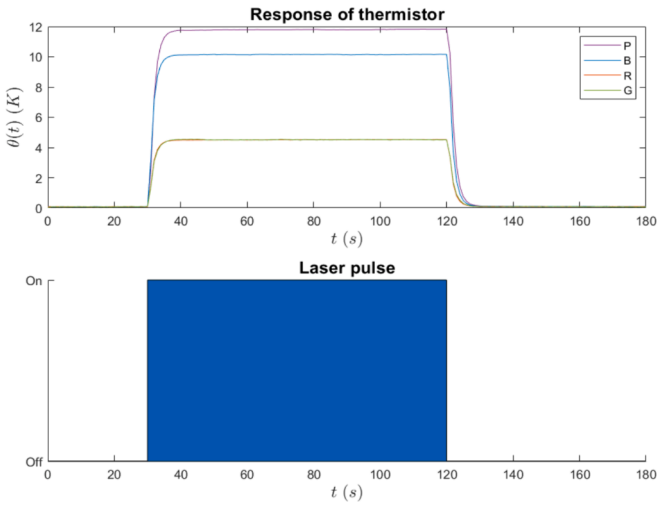

Fig. 12. Thermistor response to helium in chamber.

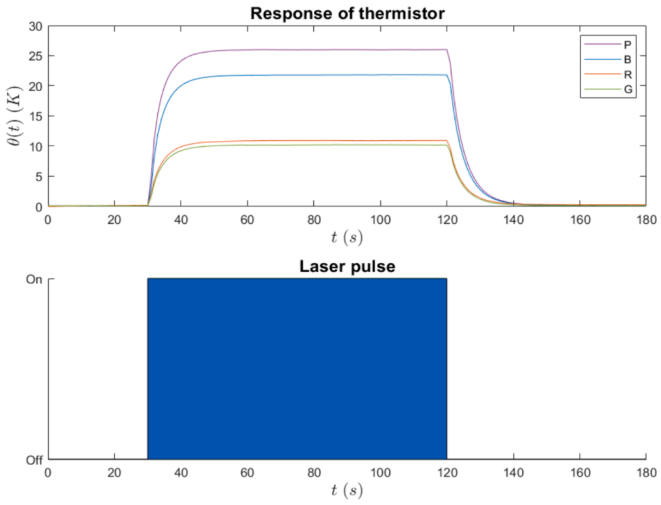

Fig. 13. Thermistor response to vacuum in chamber.

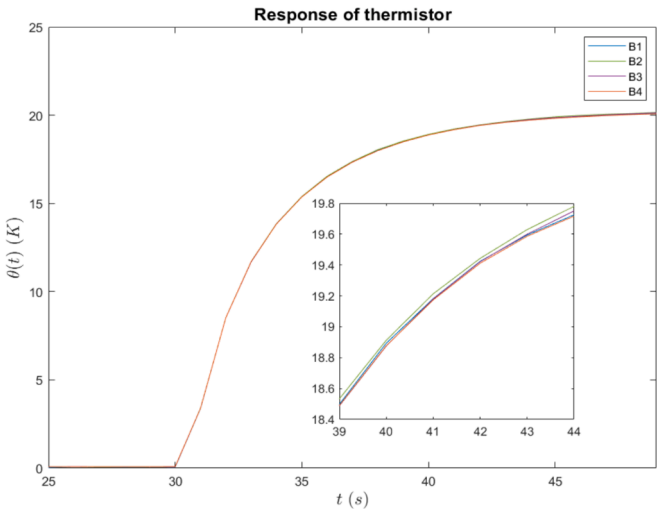

Fig. 14. Thermistor response in rising phase with ambient air in chamber.

residual values are structured in a similar manner. The first row presents the results obtained with the highest power laser (P), followed by B, R, and G for each gaseous medium. Fig. 10 illustrates the operation of the laser within the test chamber.

Finally, each test is individually presented using logarithmic temperature graphs ($\Theta(t)$). This technique enables the identification of trends across a wide range of values, thereby providing a deeper understanding of the experimental results and their implications for the behaviour of the system under study.

4.1. Thermistor transient response at different laser powers and gaseous medium characteristics

Fig. 11 illustrates the temperature thermistor responses when ambient air is used as the gas in the chamber for four different laser powers. This allows for direct analysis of the amplitude corresponding to each signal, thereby enabling an understanding of the effect of the laser power source on the temperature thermistor response. Additionally, Fig. 11 displays that the experiment commences after a stabilization period preceding the laser stimulus. For the remaining results shown in Figs. 12, 13 and 14, the behaviour of the test remains consistent.

It is worth mentioning that by monitoring the internal and external parameters, a reference measurement of the environment is available, indicating a temperature of 24 °C and a relative humidity of 45 %.

The discussion of the helium experiment follows the description of the ambient air experiment. Helium has a thermal diffusivity coefficient approximately ten times greater than that of air, which is a crucial factor to consider in experimental design. As shown in the corresponding graph.

For the vacuum tests, a pressure of −1.0 bar is achieved inside the chamber using a pump and valve system. The responses obtained are shown in the graph below (Fig. 13):

Fig. 14 presents the outcomes of four tests conducted with air under identical laser source excitation conditions. The results demonstrate the consistency and repeatability of the experimental design. The considerable overlap of results indicates minimal deviation between tests, thereby reaffirming the reliability and accuracy of the experimental design under the indicated conditions. The subsequent results of the paper exhibit a level of repeatability comparable to that presented in Fig. 14.

4.2. Fitting and comparison of the mathematical models

To assess the validity of the mathematical models considered in this paper, the time constant model (29) and the proposed improved model (27) and (28), a non-linear least squares method [31,32] is applied. The non-linear least squares method is based on the Gauss-Newton algorithm with restrictions on the model parameters using the Trust-region algorithm. The residual sums of squares or qualitative estimator (QE) data (41) are obtained from the least square process for each experiment with m samples per test. Four tests ($n = 4$) were conducted, each with different laser power settings and fluid.

$$QE = \sum_{i=1}^{m} \left(\theta_{exp\,i} - \theta_{model\,i}\right)^2 \tag{41}$$

For each laser power setting, the mean quality estimate (μ) and corresponding standard deviation (σ) were calculated for the corresponding four tests, as shown by expressions (42).

$$\mu_{QE} = \frac{\sum_{i=1}^{n} QE_i}{n} \sigma_{QE} = \sqrt{\frac{\sum_{i=1}^{n} \left(\mu_{QE} - QE_i\right)^2}{n-1}} \tag{42}$$

Furthermore, the mean (μ_{p_i}) and standard deviation (σ_{p_i}) of the proposed parameters ($p_i = \{a^*, \tau, \epsilon, \lambda, \cdots\}$) were utilized to evaluate the results of each test, as presented in expressions (43).

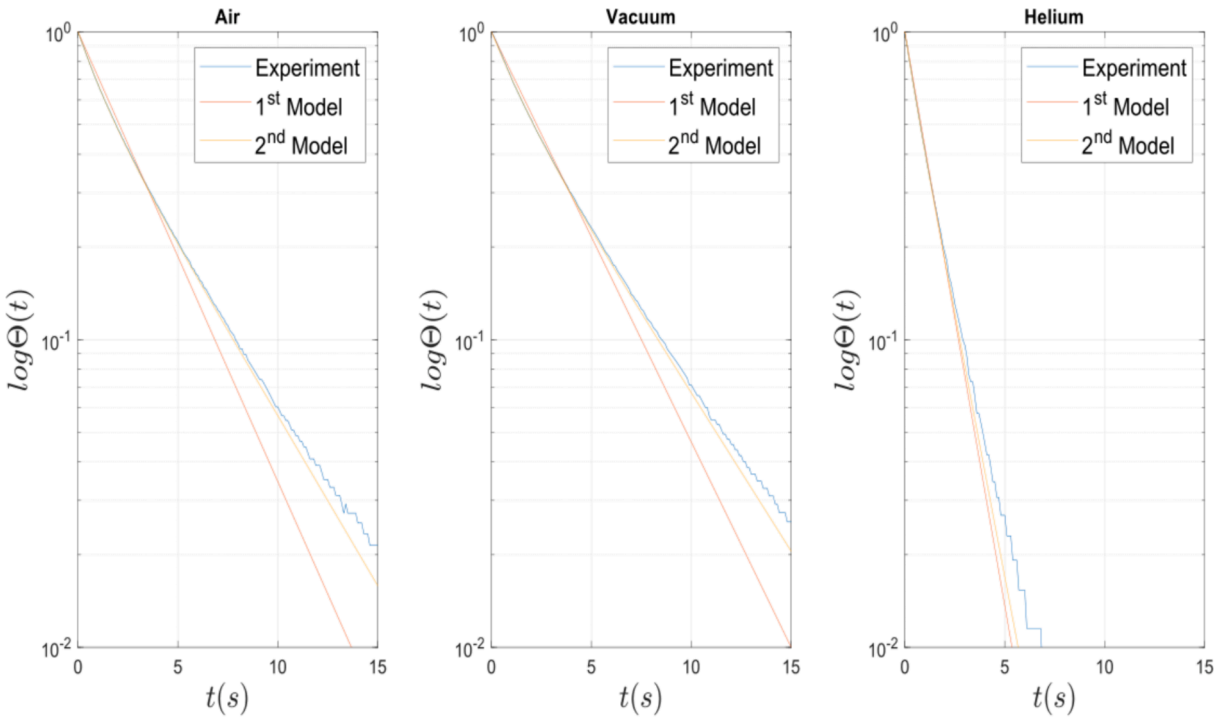

Fig. 15. Dimensionless temperature $\Theta(t)$ for laser B.

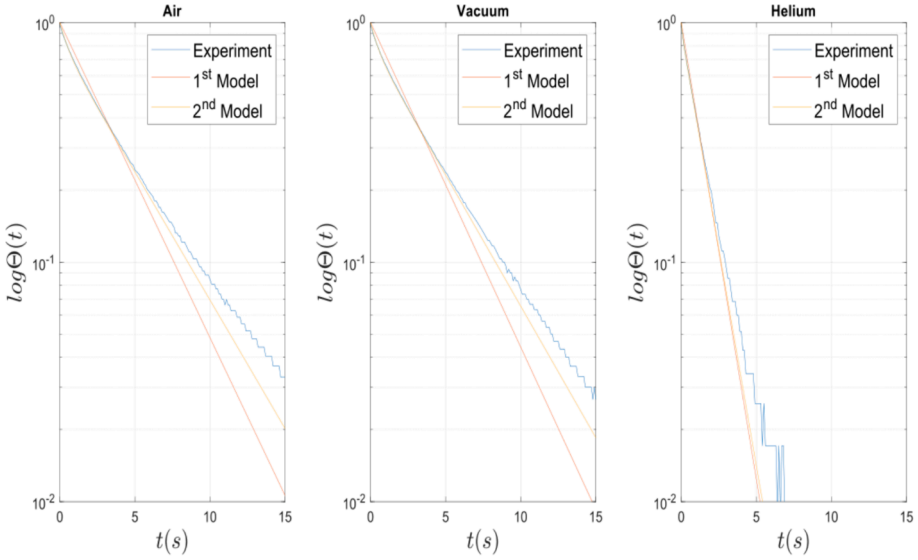

Fig. 16. Dimensionless temperature $\Theta(t)$ for laser R.

$$\mu_{p_i} = \frac{\sum_{i=1}^{n} p_i}{n} \sigma_{p_i} = \sqrt{\frac{\sum_{i=1}^{n} \left(\mu_{p_i} - p_i\right)^2}{n-1}} \tag{43}$$

In order to contrast the data provided by the thermistor manufacturer and to emphasise the importance of considering not only the properties of the sensor, but also those of the fluid to be monitored, the following tables present the results of the conventional time constant model in comparison with the results proposed in this article.

In contrast, the values of the parameters and the qualitative estimator for the proposed improved model (26) and (27) are shown in the following table 7-9:

Figs. 15 and 16 show the analysis of the model from a dimensionless perspective of the data obtained. These plots are very useful as they graphically show the existing deviations of the proposed model with respect to the experimental data. For this reason, the response of the thermistor has been analysed when the external heat source acts, taking into account the logarithm of the temperature.

Table 4
Parameters and QE values for time constant model (29) in air.

ID	*n*	a^*		τ		*QE*	
		μ_{a^*}	σ_{a^*}	μ_τ	σ_τ	μ_{QE}	σ_{QE}
P	4	25.47	0.09	2.84	0.01	73.98	1.13
B	4	20.25	0.02	3.08	0.01	35.98	2.43
R	4	10.50	0.01	3.41	0.01	14.96	0.27
G	4	9.82	0.04	3.48	0.04	12.38	0.85

Table 5
Parameters and QE values for time constant model (29) in vacuum.

ID	n	a^*		τ		QE	
		μ_{a^*}	σ_{a^*}	μ_τ	σ_τ	μ_{QE}	σ_{QE}
P	4	24.37	0.03	2.98	0.01	84.67	2.99
B	4	19.91	0.01	3.35	0.01	30.26	4.17
R	4	10.15	0.01	3.29	0.04	19.96	2.06
G	4	9.30	0.02	3.37	0.3	13.68	1.23

Table 6
Parameters and QE values for time constant model (29) in helium.

ID	n	a^*		τ		QE	
		μ_{a^*}	σ_{a^*}	μ_τ	σ_τ	μ_{QE}	σ_{QE}
P	4	11.77	0.03	1.36	0.03	2.53	0.24
B	4	10.07	0.01	1.18	0.01	1.06	0.09
R	4	4.40	0.01	1.17	0.01	0.59	0.08
G	4	4.36	0.06	1.24	0.02	4.52	0.18

5. Discussion

Tables 2 to 9 demonstrate that the proposed model in this paper (27)-(28) reduces residuals (*QE*) in comparison to the conventional model. This fact supports the hypothesis that heat flow through conductors can be relevant in temperature measurement when the dimensionless Biot number is reduced. Additionally, model (29) shows worse residuals for air than for helium, despite the expected opposite. The Biot number ($Bi = h{\cdot}D_s/k_s$) is lower for air than for helium because the average convection coefficient for helium is higher than for air under the same conditions.

It is worth noting that tables 2 to 9 confirm the sensitivity of parameters a^*, ϵ, and λ to changes in the stimulus source (P_{laser}), as expected based on the deductions made in expressions (27), (28), and (29). Similarly, considering the constants set in the mathematical models, it can be observed that the changes in laser power stimulus do not significantly affect (τ), ($\delta - \gamma$), and ($\delta + \gamma$). Appreciable variability is only observed in the case of the parameter ($\delta + \gamma$), but this could be corrected by fixing or forcing an average value for this parameter between stimuli, assuming an increase in the value of the corresponding residuals.

To discuss the effect of improving the mathematical model more precisely, a ratio (R_{QE}) of the percentage change in the average residual (μ_{QE}) between the application of the two models considered, conven-

Table 7
Parameters and QE values for the proposed improved model (27) in air.

ID	n	ϵ		λ		$(\delta+\gamma)$		$(\delta-\gamma)$		QE	
		μ_ϵ	σ_ϵ	μ_λ	σ_λ	$\mu_{\delta+\gamma}$	$\sigma_{\delta+\gamma}$	$\mu_{\delta-\gamma}$	$\sigma_{\delta-\gamma}$	μ_{QE}	σ_{QE}
P	4	25.48	0.08	−8.46	0.35	0.97	0.03	0.25	0.01	2.62	0.18
B	4	20.25	0.01	−6.76	0.68	0.79	0.06	0.23	0.01	1.27	0.45
R	4	10.50	0.01	−2.59	0.06	1.13	0.03	0.22	0.01	0.78	0.17
G	4	9.82	0.03	−2.42	0.22	0.88	0.06	0.22	0.01	4.39	0.26

Table 8
Parameters and QE values for the proposed improved model (28) in vacuum.

ID	n	ϵ		λ		$(\delta+\gamma)$		$(\delta-\gamma)$		QE	
		μ_ϵ	σ_ϵ	μ_λ	σ_λ	$\mu_{\delta+\gamma}$	$\sigma_{\delta+\gamma}$	$\mu_{\delta-\gamma}$	$\sigma_{\delta-\gamma}$	μ_{QE}	σ_{QE}
P	4	25.82	0.05	−8.83	0.28	0.96	0.02	0.24	0.01	1.88	0.07
B	4	21.69	0.03	−9.31	1.01	0.55	0.02	0.21	0.01	1.01	0.49
R	4	11.56	0.02	−2.64	0.19	1.44	0.10	0.23	0.01	0.94	0.28
G	4	10.09	0.04	−2.05	0.96	0.78	0.04	0.23	0.05	3.57	0.31

Table 9
Parameters and QE values for the proposed improved model (27) in helium.

ID	n	ϵ		λ		$(\delta+\gamma)$		$(\delta-\gamma)$		QE	
		μ_ϵ	σ_ϵ	μ_λ	σ_λ	$\mu_{\delta+\gamma}$	$\sigma_{\delta+\gamma}$	$\mu_{\delta-\gamma}$	$\sigma_{\delta-\gamma}$	μ_{QE}	σ_{QE}
P	4	11.77	0.03	−11.65	0.35	0.68	0.005	0.69	0.01	2.59	0.15
B	4	10.07	0.01	−4.56	0.32	1.31	0.03	0.63	0.02	0.27	0.06
R	4	4.40	0.01	−0.89	0.11	2.65	0.33	0.71	0.01	0.26	0.03
G	4	4.36	0.06	−0.84	0.30	2.34	0.53	0.67	0.05	4.24	0.12

Table 10
Average and relative variation of QE values per model and power laser.

	Air			Vacuum			Helium		
	μ_{QE}		R_{QE}	μ_{QE}		R_{QE}	μ_{QE}		R_{QE}
Model	**(29)**	**(27)**	**%**	**(29)**	**(28)**	**%**	**(29)**	**(27)**	**%**
P	77.4	2.6	3.4	84.31	1.88	2.2	3.8	2.6	68.9
B	37.2	1.3	3.4	28.73	1.01	3.5	1.1	0.3	25.5
R	15.1	0.8	5.2	19.22	0.94	4.9	0.7	0.3	37.7
G	13.3	4.4	32.9	14.15	3.57	25.2	9.8	4.2	43.4
Average	35.7	2.3	11.2	36.6	1.9	9.0	3.8	1.8	43.8

tional (29) and proposed (27) or (28), is defined by the expression (44).

$$R_{QE} = \frac{\mu_{QE}(i)}{\mu_{QE}(29)} \cdot 100i = \{27, 28\} \quad (44)$$

Table 10 presents a comparative summary of the results from the different adjustments displayed in tables 2 to 9. The summary includes the residual or estimator of the quality of fit of the models considered QE, as well as the values of the rate of change ratio (44).

It is clear from Table 10 that the results can be improved by approximating the heat flow through the wires. This is particularly true for air and vacuum, and to a lesser extent for the helium case. Improvements in the average model fit are of the order of 89 % for air, 91 % for vacuum and 56 % for helium. It should be noted that only the simplest approximation (19) was used to estimate the wire heat flux. It is expected that the use of a more complex approximation, such as (20), would lead to further improvements. However, the results indicate that heat exchange through the sensor wires does affect the measurement.

Figs. 15 and 16 confirm the previous indication that the proposed model gives better results than the conventional one. The presentation of the results in dimensionless form is effective after applying the appropriate logarithmic scale change.

6. Conclusions

This work proposes a mathematical model that incorporates the transient response of thermistors characterised by a synergy between the gaseous medium and the sensor, which results in a low Biot number ($Bi < 0.1$), mainly in applications where the interaction with the studied phenomenon is minimal. This strategy complements the conventional model based on the concept of time constant. The improvement assumes that the heat flow through the thermistor wires must be considered in the energy balance, treating them as semi-infinite solids and applying an approximation to their heat flow formula. Additionally, an approach based on the use of equivalent transfer functions has been applied to the mathematical model of semi-infinite solids, maintaining simplicity for the required level of accuracy. The proposed model has been validated against experimental results, demonstrating superior performance compared to the conventional time constant model. The improvements in the average model fit are approximately 89 % for air, 91 % for vacuum and 56 % for helium. These results indicate a satisfactory enhancement over the conventional model, suggesting that heat exchange through the sensor wires significantly affects the measurement.

CRediT authorship contribution statement

Jorge Valencia-Santana: Writing – original draft, Software, Resources, Methodology, Investigation. **Alejandro Ramos-Martín:** Writing – review & editing, Validation, Supervision. **Vicente Henríquez-Concepción:** Writing – review & editing, Supervision.

Declaration of competing interest

The authors declare that they have no known competing financial interests or personal relationships that could have appeared to influence the work reported in this paper.

Data availability

Data will be made available on request.

References

[1] S. Rudtsch, C. von Rohden, Calibration and self-validation of thermistors for high-precision temperature measurements, Measurement 76 (2015) 1–6, https://doi.org/10.1016/j.measurement.2015.07.028.

[2] G. Liu, L. Guo, C. Liu, Q. Wu, Evaluation of different calibration equations for NTC thermistor applied to high-precision temperature measurement, Measurement 120 (2018) 21–27, https://doi.org/10.1016/j.measurement.2018.02.007.

[3] V.C.V. Santos, T.L.M. Santos, On the variance propagation of thermistor-based measurements with a digital temperature controller, Measurement 192 (2022) 110863, https://doi.org/10.1016/j.measurement.2022.110863.

[4] J. Kim, J.D. Kim, Voltage divider resistance for high-resolution of the thermistor temperature measurement, Measurement 44 (10) (2011) 2054–2059, https://doi.org/10.1016/j.measurement.2011.08.004.

[5] D. Ross-Pinnock, P.G. Maropoulos, Review of industrial temperature measurement technologies and research priorities for the thermal characterisation of the factories of the future, Proc Inst Mech Eng B J Eng Manuf 230 (2016) 793–806, https://doi.org/10.1177/0954405414567929.

[6] H. E. Darkhaneh, "Measurement error caused by self-heating in NTC and PTC thermistors," Dallas, Texas, 2019. Accessed: Mar. 02, 2024. [Online]. Available: https://api.semanticscholar.org/CorpusID:203587887.

[7] J. Fraden, Handbook of Modern Sensors. Physics, designs and applications, Fifth Edition. Springer (2015), https://doi.org/10.1007/978-1-4419-6466-3.

[8] J.-L. Gardarein, J.-L. Battaglia, S. Löhle, Heat flux sensor calibration using noninteger system identification: Theory, experiment, and error analysis, Rev. Sci. Instrum. 80 (2) (Feb. 2009) 025103, https://doi.org/10.1063/1.3079328.

[9] H. Wang, et al., Fast response characteristics of fiber Bragg grating temperature sensors and explosion temperature measurement tests, Sens Actuators A Phys 354 (2023) 114236, https://doi.org/10.1016/j.sna.2023.114236.

[10] Q. Wang, W. Kong, J. Yao, A. Chang, Fabrication and electrical properties of the fast response Mn1.2Co1.5Ni0.3O4 miniature NTC chip thermistors, Ceram Int 45 (1) (2019) 378–383, https://doi.org/10.1016/j.ceramint.2018.09.177.

[11] S.L.N. Desikan, K. Suresh, K. Srinivasan, P.G. Raveendran, Fast response co-axial thermocouple for short duration impulse facilities, Appl Therm Eng 96 (2016) 48–56, https://doi.org/10.1016/j.applthermaleng.2015.11.074.

[12] Y.A. Cengel, Heat transfer. A practical approach, Second edition, McGraw-Hill, New York (NY), 2002.

[13] G.M. Carlomagno, L. de Luca, G. Cardone, T. Astarita, Heat flux sensors for infrared thermography in convective heat transfer, Sensors (switzerland) 14 (11) (Nov. 2014) 21065–21116, https://doi.org/10.3390/s141121065.

[14] M. Tagawa, K. Kato, Y. Ohta, Response compensation of thermistors: Frequency response and identification of thermal time constant, Rev. Sci. Instrum. 74 (3) (Mar. 2003) 1350–1358, https://doi.org/10.1063/1.1542668.

[15] D. B. Spalding, "Heat Transfer. By Alan J. Chapman. The Macmillan Company, New York. 1960. 452pp. 63s.," *J Fluid Mech*, vol. 10, no. 2, pp. 317–319, 1961, doi: DOI: 10.1017/S002211206122026X.

[16] O.G. Martynenko, R.I. Soloukhin, Heat conduction: M. N. Ožišik, John Wiley, New York (1980). 687 pp, Int J Heat Mass Transf 24 (12) (Dec. 1981) 1993–1994, https://doi.org/10.1016/0017-9310(81)90124-1.

[17] D. Maillet, S. André, J.C. Batsale, A. Degiovanni, C. Myoyne, Thermal Quadrupoles: Solving the Heat Equation through Integral Transforms. (2000).

[18] R. Heyd, One-Dimensional Systemic Modeling of Thermal Sensors Based on Miniature Bead-Type Thermistors, Sensors 21 (23) (Nov. 2021) 7866, https://doi.org/10.3390/s21237866.

[19] V. D. Beybalaev, A. A. Aliverdiev, and J. Hristov, "Transient Heat Conduction in a Semi-Infinite Domain with a Memory Effect: Analytical Solutions with a Robin Boundary Condition," *Fractal and Fractional*, vol. 7, no. 10, 2023, doi: 10.3390/fractalfract7100770.

[20] K. B. Oldham and J. Spanier, *The Fractional Calculus. Theory and Applications of Differentiation and Integration to Arbitrary Order*, first. California: Academic Press, INC.

[21] TDK Group Company, "NTC Thermistors. General technical information," Nov. 2012. Accessed: Jun. 11, 2023. [Online]. Available: https://www.tdk-electronics.tdk.com/download/531116/19643b7ea798d7c4670141a88cd993f9/pdf-general-technical-information.pdf.

[22] M. Necati. Özışık, "Heat transfer: a basic approach," p. 780, 1985.

[23] J.I. Sylvia, S.C.R. Chandar, K. Velusamy, A novel method for in-situ estimation of time constant for core temperature monitoring thermocouples of operating reactors, Nucl. Eng. Des. 275 (2014) 154–162, https://doi.org/10.1016/j.nucengdes.2014.04.007.

[24] Y. Jannot, C. Moyne, and A. Degiovanni, *Heat Transfer, Volume 1: Conduction and Convection*, Second., vol. 1. Wiley, 2023.

[25] D. Wu, Y. Tao, H. Ren, The Laplace Transform Shortcut Solution to a One-Dimensional Heat Conduction Model with Dirichlet Boundary Conditions, Axioms 12 (8) (2023) Aug, https://doi.org/10.3390/axioms12080770.

[26] J. Taler P. Duda Solving Direct and Inverse Heat Conduction Problems 2006 Springer Berlin Heidelberg 10.1007/978-3-540-33471-2.

[27] G.E. Carlson, "Approximation of Fractional Capacitors (1/s)^(1/n) by a Regular Newton, Process" (1960).

[28] G. E. Carlson, "Simulation of the Fractional Derivative Operator and the Fractional Integral Operator," Kansas State University, 1960. Accessed: Mar. 02, 2024. [Online]. Available: http://hdl.handle.net/2097/16007.

[29] B.M. Vinagre, I. Podlubny, A. Hernandez, V. Feliu, Some approximations of fractional order operators used in control theory and applications, Fract Calc Appl Anal 3 (2000) 231–248.

[30] I. Podlubny I. Petráš B.M. Vinagre P. O'leary, and L'. Dorˇ Cák, Analogue Realizations of Fractional-Order Controllers Nonlinear Dyn 29 2002 281 296.

[31] M. A. Jacroux, "A non-least squares approach to linear models," p. 192.

[32] G. Chavent, "Nonlinear Least Squares for Inverse Problems," 2010, doi: 10.1007/978-90-481-2785-6.